Mechanical characterization of anisotropy on a carbon fiber sheet molding compound composite under quasi-static and fatigue loading

C Nony-Davadie[1], L Peltier[1], Y Chemisky[1], B Surowiec[2] and F Meraghni[1]

Abstract

The paper presents an experimental analysis of the anisotropic effects of the structural advanced carbon fiber sheet molding compound composites (AC-SMCs) subjected to quasi-static and fatigue loading. Two configurations of AC-SMC composites (randomly oriented and highly oriented) considering three different orientations (0°, 45°, 90°) with respect to the material thermo-compression flow direction are investigated under quasi-static and fatigue tensile loading. The effects of fibers orientation induced by the thermo-compression process are analyzed in terms of ultimate strength, elastic modulus, and macroscopic damage corresponding to the stiffness reduction, and related to the quasi-static and fatigue behavior. For both loading conditions, the macroscopic damage of AC-SMC randomly oriented exhibits a two-stage evolution without any damage saturation prior to the samples' failure. In addition, the difference between the highly oriented and randomly oriented configurations is pronounced especially for the 45° and 90° orientations. Post-mortem X-ray radiography and SEM observations show that damage mechanisms such as microcracks appear between and inside bundles, and their occurrence depends on the sample orientation. Experimental findings are compared with those of an equivalent advanced glass fiber reinforced sheet molding compounds composite. The degree of anisotropy is more pronounced for AC-SMC. Indeed, the dependency of the behavior during the manufacturing process induces orientation. Furthermore, the damage evolutions of the two types of SMCs have displayed different kinetics, especially for the saturation stage which is not observed for the AC-SMC composite.

Keywords

Carbon sheet molding compound composite, short bundles reinforcement, damage mechanisms, anisotropy, microstructures, mechanical testing, fatigue

Introduction

Sheet molding compounds (SMCs) materials are widely employed in the automotive industry due to their high strength-to-weight ratio and their flexibility.[1–3] Those features make them ideal candidates for large semi-structural automotive components. Driven by the need of car manufacturers to improve the mechanical performances of their vehicles, high-fiber content of SMCs composite has been developed by Plastic Omnium.[4,5] Thanks to the vinyl-ester thermoset resin; those advanced sheet molding compounds (A-SMCs) allow a higher content of reinforcement. Classical SMC[3,6–8] have a fiber content below 35% weight when the developed vinyl-ester resin allows a reinforcement weight content up to 60% weight. Such improvement offers new perspectives in terms of applications, especially in the automotive industry. Further developments were next conducted: on the one hand by improving the compound with the addition of hollow glass spheres to produce a low-density SMC,[9] on the

[1]LEM3-UMR CNRS 7239-Arts et Métiers ParisTech, France
[2]Plastic Omnium Auto Exterior, Sigmatech, France

Corresponding author:
F Meraghni, Arts et Metiers ParisTech – Centre de Metz 4 Rue Augustin FRESNEL, Metz 57078, France.
Email: fodil.meraghni@ensam.eu

other hand by substituting the bundles of glass fibers by carbon fibers ones, to increase the mechanical properties, especially the stiffness-to-density ratio. Such improvement is particularly important for structural applications. Indeed, typical applications for SMC in the automotive industry are semi-structural parts with no or limited safety function, such as rear floor. Thanks to the potential offered by A-SMC reinforced with carbon fibers bundles, the automotive industry might move toward fully load-bearing structure made of composite materials.[10] Indeed, carbon fiber molding compounds reinforced epoxy matrix have been developed in 2003 by the European resin-produced DSM dedicated to semi-structural automotive components. The flow characteristics of low-cost carbon fiber molding compounds reinforcing epoxy matrix has been studied using an automated spray deposition process.[11] The effect of several material and process parameters have been analyzed in relation with the level of macroscopic reinforcement flow and compared to the characteristic flow of conventional glass fiber SMCs. Another recent study has been devoted to the quality assessment of the molded parts and semi-finished (carbon fiber tows) material made of SMC with unidirectional (UD) carbon fiber tapes. The authors applied two techniques, thermography and ultrasound, for identifying process-induced defects (misaligned fibers and microstructural changes, air inclusions, delamination).[12]

Following the designation proposed by Shirinbayan et al.,[4,5] this new class of SMC is referred to as advanced carbon-sheet molding compound (AC-SMC). Hence, the combination of vinyl-ester thermoset resin and short bundles of carbon fibers has a higher ratio of stiffness-to-density than steel. However, the use of AC-SMC composites in critical automotive components requires an extensive fatigue analysis, especially with the identification of the damage mechanisms, failure modes, and the impact of mechanical loading and environment on their fatigue life.

Extensive research has been pursued concerning the analysis of the mechanical behavior of SMC.[4,5,13–15] Denton[13] characterized the mechanical response of an SMC as a function of temperature under quasi-static (QS) and cyclic loading, while Wang and Chim[14] studied the effect of fatigue on the degradation of a randomly oriented (RO) SMC and identified different damage mechanisms. Hour and Sehitoglu[15] focused their work on the estimation of the damage volumetric strain. A recent experimental work by Trauth et al.[16] has been devoted to the effect of anisotropic fiber orientation and orientation-dependent mechanical properties on the mechanical behavior of glass fiber reinforced vinyl-ester-based SMC. The authors have shown that the process-induced fiber orientation affects the QS and dynamic material properties. More recently, Shirinbayan et al. studied the effect of high strain rate loading[4] and the effect of loading frequency[5] on the damage behavior of an A-SMC with respect to loading orientation. Despite a non-viscous elastic behavior, high-speed loading experiments have highlighted that the damage mechanisms are the same for all directions. Further, the more the strain rate increase, the more the phenomena of pseudo-delamination of bundles is promoted, displaying a viscous damageable behavior. As frequency increased, a significant self-heating has been observed, leading to a shortening of fatigue life.

According to their production and use for automotive applications, AC-SMCs are subjected to QS and fatigue loadings. To design components that can bear fatigue loading, the damage mechanisms of AC-SMC composites, and their effect, should be identified and characterized. Fatigue life is usually characterized by an S-N curve drawn from a combination of QS and cyclic tests, from which one may extract the Wöhler curve.[17,18] To properly estimate the fatigue life of short bundles reinforced polymer composites, various characteristics have to be taken into account. The process-induced microstructure and the reinforcement orientation,[4,5] nature of the matrix,[17] mean stress,[14] loading frequency, temperature, and humidity are the main ones. It is worth noticing that in the open literature few papers have been published on the mechanical characteristics of carbon fiber reinforced vinyl-ester-based SMC. One can cite the work of Ogi et al. devoted to (1) the impact damage and residual strength[19] and (2) the effect of temperature on flexural strength.[20] Recently, a relevant paper has been published by Trauth et al.[21] It deals with the experimental investigation of the mechanical properties and the damage mechanisms of a hybrid (carbon-glass reinforcement) SMC based on a two-step curing resin system.

The present study is dedicated to the experimental analysis of the QS and the cyclic mechanical behavior of AC-SMCs as well as the related damage mechanisms and fatigue failure modes in two AC-SMC configurations. The paper presents an experimental methodology devoted to the analysis of the anisotropic effects of the AC-SMC composites induced by the thermo-compression process. The experimental findings obtained on two configurations of AC-SMC composites (namely randomly oriented (RO) and highly oriented (HO)) under QS and fatigue loading conditions have been compared with those of an equivalent glass fiber reinforced A-SMC.

The paper is organized as follows: the second section describes the AC-SMC composite material as well as the process-induced microstructure and the experimental procedure and methods used in order to characterize the mechanical behavior of the AC-SMC and the damage evolution under QS and tension-tension

fatigue loading, to identify the various damage mechanisms evolution. Then, in the Experimental Results and Discussion sections, the results will be presented, discussed in terms of microstructure orientation and loading ratio effects, and compared with the published results on A-SMC by Shirinbayan et al.[4,5] Finally, in the concluding section, the main experimental findings are summarized to highlight the features of the AC-SMC and the effects of process-induced microstructure on the macroscopic mechanical response of the composite.

Material description and experimental methods

AC-SMC

AC-SMC consists of vinyl-ester thermoset matrix reinforced by short carbon bundles having a length of 25.4 mm (Figure 1). According to the thermo-compression process, the bundles present a specific orientation. The studied AC-SMC contains a high overall content of carbon reinforcement (55% in weight ratio, corresponding to 44.9% in volume ratio), as summarized in Table 1. It should be pointed out that the AC-SMC does not contain fillers, contrary to classical A-SMC.

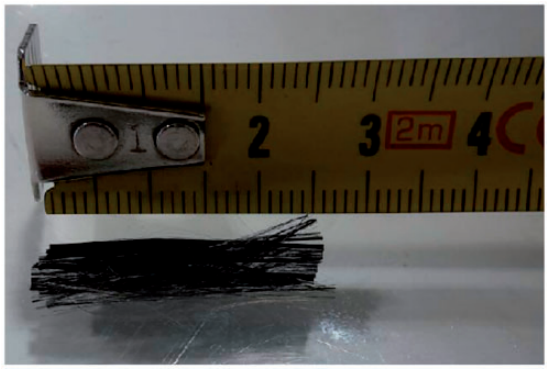

Figure 1. Carbon bundle extracted from the semi-product sheet molding compound (SMC) sheets before thermo-compression. The carbon bundle consists of UD oriented fibers with a length of 25.4 mm.

Table 1. Advanced carbon-sheet molding compound (AC-SMC) composition and constituents' weight content.

Composition	Content (in weight ratio)
Vinyl-ester resin	43%
Carbon fiber bundles	55%
Additives	2%

Indeed, since carbon fibers have a smaller diameter ($\phi_{carbon} = 7\mu m$) compared to glass fiber ones ($\phi_{glass} = 15\mu m$) a lower viscosity is required to impregnate them.

The manufacture of a consolidated AC-SMC plate can be made up of two process stages.[22] During the first stage the paste reservoir dispenses a measured amount of specified resin paste onto a plastic carrier film. This carrier film passes underneath a chopper which cuts the bundles of fibers onto the surface. Once these have drifted through the depth of resin paste, another sheet is added on top which sandwiches the carbon bundles. The sheets are compacted and then enter onto a take-up roll, which is used to store the product whilst it matures. During the second stage, the carrier film is then removed and the material is cut into patterns. The shape of the pattern is determined according to the shape of the mold and the process parameters. Matched metal dies are mounted in a hydraulic molding press. The material pattern is manually or robotically placed in the mold, the heated mold halves are closed, 80 bar of pressure and a temperature of 150°C is applied. Cycle time ranges from 1 to 2 min depending on part size and thickness. It should be mentioned that there are also other existing SMC processes such as chopped fiber reinforcement and resin sprayed directly dosed into the mold.[11]

Qualitative investigation of the AC-SMC microstructure has been carried out using an optical microscope (Zeiss Axio). From such micrographs, two subscales are observed: the microscale, in which the fibers and the matrix compose a single bundle (Figure 2(a)), and the mesoscale, where multiple bundles are embedded in the matrix in various orientations on the thermo-compression plane (as seen in Figure 2(b)). The bundles are made of 12,000 carbon fibers Toray T300 with constant length of $L = 25.4$ mm and diameter of $d = 7\,\mu m$. The bundles are considered as UD composites with fibers volume fraction of 52.0%. The concentration of reinforcement is characterized by two values: the first is the local fibers concentration $c_{f/b}$, which represent the volume fraction of fibers in bundles ($c_{f/b} = 52.0\%$); the second $c_{b/SMC}$, which represents the volume fraction of bundles in the composite ($c_{b/SMC} = 86.3\%$). The fabrication process of the total fiber content is assumed to be constant.

$$c_{f/SMC} = c_{f/b} * c_{b/SMC} = 44.9\% \quad (1)$$

In order to investigate the effect of the process-induced microstructure, two configurations of composites plates were produced and tested, namely: RO and HO plates ($500 \times 500\,mm^2$). Both configurations are manufactured from the same batch of raw AC-SMC, with the same quantity of constituents, and are

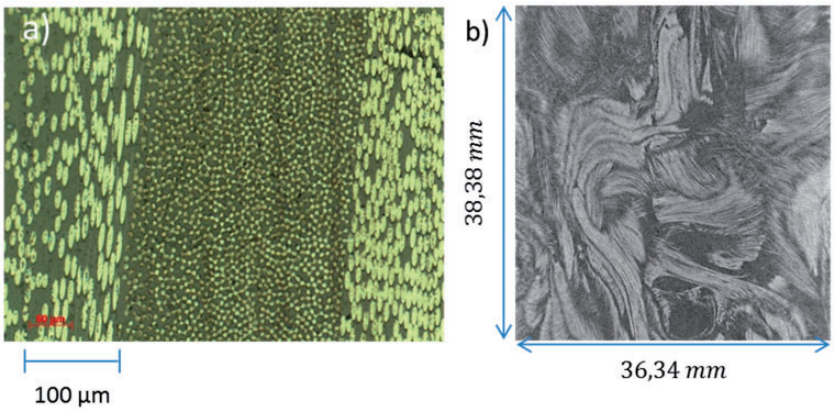

Figure 2. Typical microstructure of an AC-SMC randomly oriented observed with an optical microscope, (a) detail of the fiber microstructure within bundle and (b) overall microstructure.
AC-SMC: advanced carbon-sheet molding compound.

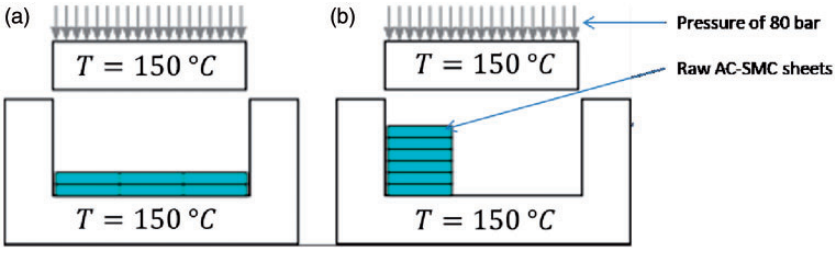

Figure 3. Schematic of the initial mold surface coverage during the thermo-compression process: (a) case of SMC RO and (b) case of SMC HO. The mold filling process governs the material flow and induces specific microstructures.
SMC: sheet molding compound; RO: randomly oriented; HO: highly oriented.

processed by thermo-compression under the same manufacturing conditions; their sole difference arises from the mold-filling process. For the RO configuration, the initial mold surface is covered at 97% with two layers of semi-product SMC sheets centered within it (Figure 3(a)). This filling mode permits to preserve the initial sheets' microstructure, which is considered isotropic in the sheet plane. However, in the case of the HO one, the objective is to highly reorient the raw microstructure in a privileged direction during the thermo-compression. As a consequence, the two layers are cut in three equal pieces which are then stacked on one side of the mold, reducing the initial mold surface coverage to 32.3%. Resulting from this stacking, the material will flow in one main flow direction (MMFD), changing the microstructure (Figure 3(b)). To ensure that the material flow during forming does not compensate a possible initial privileged orientation in the raw material, the sheet production direction and the main material flow direction are the same.

Specimens and experimental procedure

Sample geometry. In order to reduce the scattering of the results, to avoid that the sample break within the grips, and to maximize the number of sample cut per plate, we used dog-bone samples as presented in Figure 4(a). The dimensions of the Zone of Interest (ZoI) are, respectively, 60 mm for the length, 30 mm for the width, and a thickness of 2.2 mm. All the samples were cut using hyperbaric water jet from the manufactured plates. As presented in Figure 4(b), all specimens were extracted from a zone sufficiently far from the edges of the manufactured plate. Furthermore, it must be pointed out that the gauge zones (ZoI) of the machined specimens are positioned in the central part of the plate avoiding the ejection marks.

Experimental procedures. All performed tests (QS and fatigue) were done at room temperature and ambient humidity. In order to investigate the effect of the microstructure induced by the process (reinforcement orientation) on both AC-SMC configurations, three loading directions with respect to the "Main Material Flow Direction" (MMFD, Figure 5) were investigated.

QS tensile tests were carried out at a strain rate of $\dot{\varepsilon} = 10^{-3}s^{-1}$, on a Zwick Universal mechanical test machine. The load level was measured by a load cell having a capacity of 50 kN with an accuracy of 0.5% of the full-scale capacity. The displacement was measured

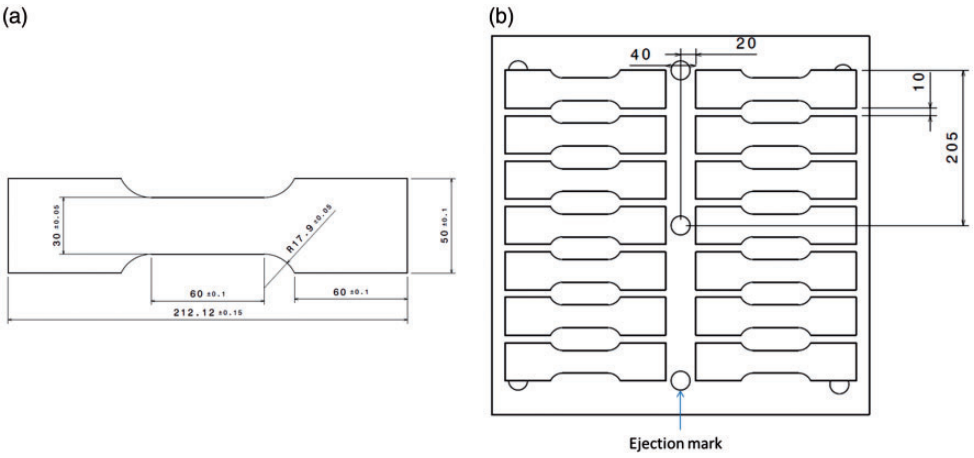

Figure 4. (a) Dog bone geometry of the tested specimen under quasi-static tension and tension–tension fatigue loading, and (b) geometrical arrangement of the waterjet cut dog-bone specimen within an AC-SMC plate.
AC-SMC: advanced carbon-sheet molding compound.

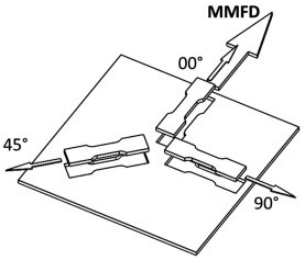

Figure 5. Three loading angles with respect to MMFD during forming.
MMFD: main material flow direction.

by Digital Images Correlation using VIC 2D software from pictures recorded by a CCD camera. The tension loading was displacement (strain)-controlled up to a given stress level. The specimens were then unloaded at the same strain rate until a load level of 0.33 MPa to avoid a potential compression state. This strain-controlled loading-unloading process was repeated by increasing incrementally the stress level with a step of 20 MPa, up to failure (Figure 6). For each loading orientation, five samples were tested.

Tension–tension fatigue tests were performed under load control at a frequency of $f = 10$ Hz, on an Instron servo-hydraulic test machine with control software. The load level is measured by a strain-gauges load cell having a capacity of ± 100 kN with an accuracy of 0.5% of the full-scale capacity. The temperature evolution is monitored by means of an infra-red (IR) camera positioned in front of the gripped specimen, as illustrated in Figure 7. The strains are computed using (1) the displacement measured by the embedded LVDT sensor within the servo hydraulic jack, and (2) the DIC technique. For the RO AC-SMC configuration, three different loading directions with respect to MMFD $\{00^{\circ}; 45^{\circ}; 90^{\circ}\}$ are considered, whereas for the HO AC-SMC configuration only one direction $\{00^{\circ}\}$ is tested. Indeed, the 0° orientation of the HO AC-SMC configuration represents the upper limit in terms of QS and fatigue behavior. Furthermore, it is worth noticing that the HO configuration of the studied advanced carbon-based SMC (HO AC-SMC) has been developed by Plastic Omnium to be employed for structural automotive components submitted to loading oriented in 0°, namely in the reinforcement direction. Conversely to that, the RO AC-SMC configuration is mainly devoted to components or partial regions of a component that are subjected to "off-axis" loading conditions.

Fatigue tests have been carried out at a loading ratio $R_{\sigma} = \frac{\sigma_{min}}{\sigma_{max}}$ equal to 0.1, which is largely considered by car manufacturers and their equipment suppliers and selected in other studies on SMC (reinforced with glass fibers).[5]

The modulus reduction has been estimated experimentally at specific defined cycles during the elastic release stage as proposed by Brunbauer et al.[23] (Figure 8). As illustrated in this figure, such procedure provides the cycle-dependent stiffness evolution. For each load levels five to nine samples were tested.

Experimental results and discussion

The main objective of this section is to investigate the effects of the manufacturing process-induced anisotropy on the mechanical response of the AC-SMC composites. Post-mortem analyses by the means of radiography and SEM observations were conducted to characterize qualitatively the degradation modes. For each loading configuration, namely QS and fatigue

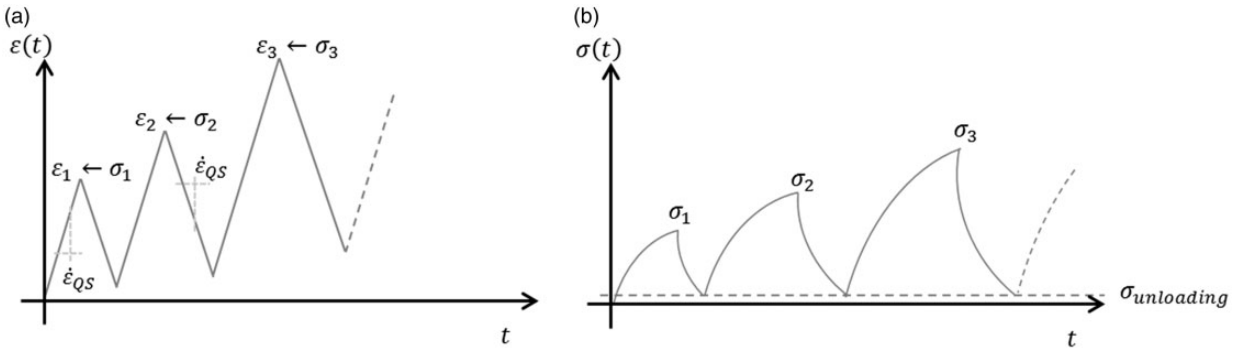

Figure 6. Qualitative representation of: (a) incremental strain-controlled loading-unloading process during the tensile tests, and (b) the schematic expected non-linear stress response evolution with respect to time.

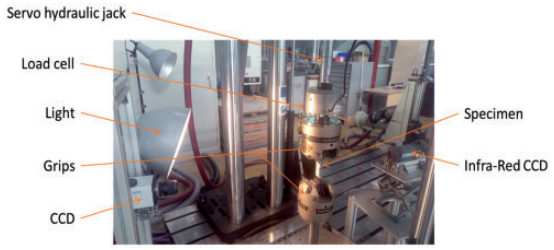

Figure 7. Testing bench and measurement devices for tension–tension cyclic tests.

tests, the obtained experimental findings have been compared with those published by Shirinbayan et al.,[4,5] with glass-based A-SMC. The presented results refer to tested samples that failed within the ZoI. Furthermore, it should be pointed out that the presented experimental results were normalized due to industrial confidentiality.

QS tensile behavior

Effect of orientation. Figures 9 and 10 illustrate the typical responses for RO and HO microstructures for three different loading directions. Tables 2 and 3 summarize the three characteristic mechanical properties for both configurations and the three loading directions: (1) E is the averaged elastic modulus of the tested considered batch of samples during the first loading, (2) σ_uts the averaged ultimate tensile stress, and (3) ε_f^l the averaged strain at failure in the longitudinal direction. The elastic modulus is estimated for every single sample between 0.05% and 0.2% of the measured strain according to the standard ISO 527. For each considered mechanical properties, the coefficient of variation is also computed.

Given the respective mold filling, it is expected an in plane isotropic behavior for the AC-SMC RO, which means that the $(\sigma - \varepsilon)$ responses should be independent of the plane loading direction. However, the experimental findings highlight certain plane anisotropy of the overall behavior, especially for the non-linear stages and on the ultimate stress and strain. Indeed, as illustrated in Figure 9, the sample loaded at 0° direction with respect to the MMFD behaves as an elastic quasi-brittle medium: high initial stiffness and ultimate stress, limited non-linear behavior, total strain at failure below 1% and almost no inelastic permanent strain after unloading. At 45°, the material exhibits a slightly higher ductility: the ultimate stress decreases by 28%, the strain to failure extends by 58%, and the inelastic permanent strain is about two times larger compared to the 0° loaded samples. The AC-SMC RO-90° samples exhibit a slightly more pronounced ductility which corresponds to an increase of strain to failure of 13% and a decrease of 27% of the ultimate stress compared to the MMFD direction. Furthermore, one notices an increase by 100% of the inelastic permanent strain compared to 45° configuration. It should be pointed out that the loading direction affects less the elastic properties. In fact, as given in Table 2, the maximum difference between the averaged elastic modulus for the three configurations does not exceed 28%.

The AC-SMC RO anisotropic behavior might not be caused by the thermo-compression molding of the composite but by the sheet manufacturing process. Since it has been assumed that (1) for the RO configuration no privileged flow direction exists during the thermo-compression process and (2) the raw sheet rolling direction coincides with 00° (MMFD), the observed plane anisotropy is associated to the SMC sheet manufacturing.

For the AC-SMC HO configuration, as expected, strong anisotropic plane behavior is highlighted (Figure 10). The stress–strain response is strongly dependent on the loading direction. At 00°, the behavior is elastic-brittle with a high initial elastic modulus and almost no damage occurs. At 45°, the material exhibits a non-linear response and the ultimate stress decreases by 57%, whereas the elastic modulus decreases by 35% compared to the 0° loaded samples.

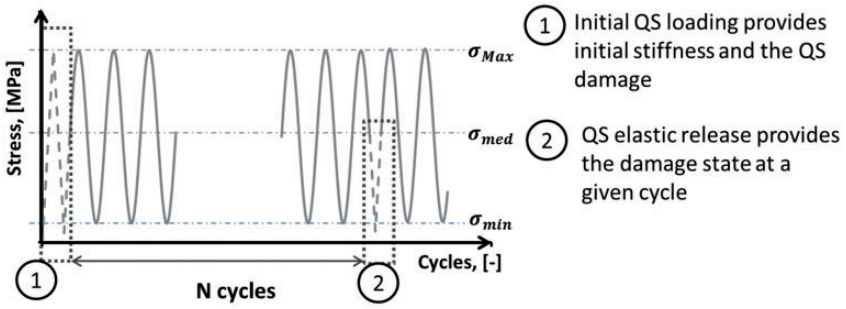

Figure 8. Testing bench for tension–tension cyclic tests.

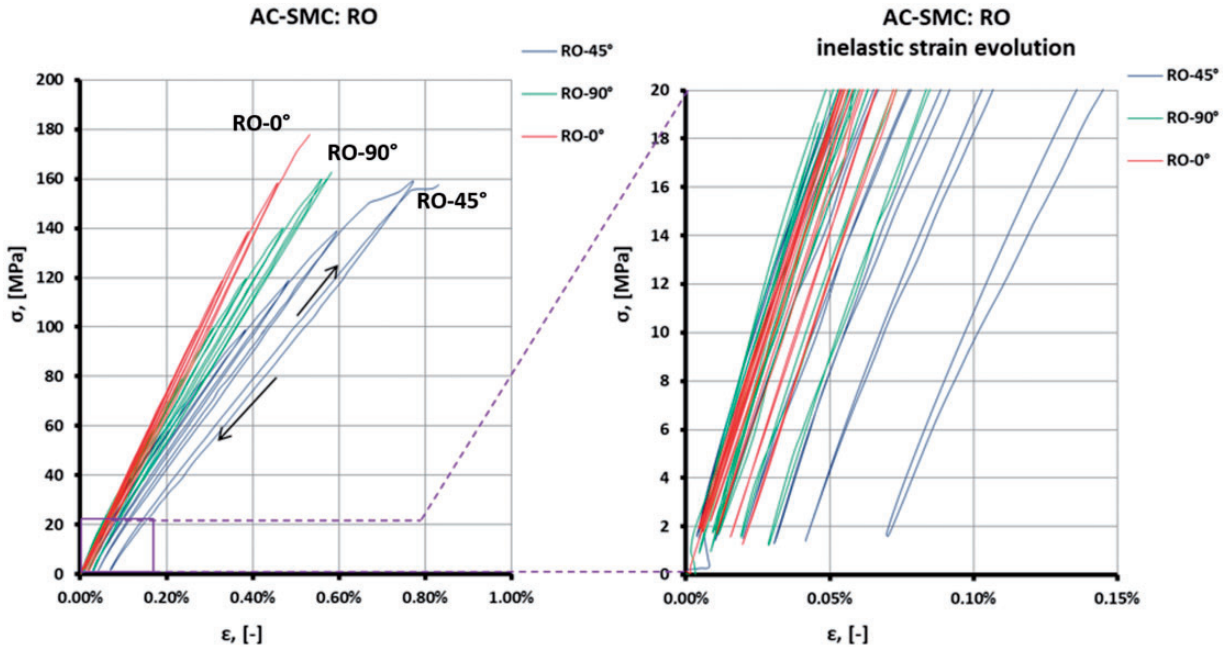

Figure 9. Quasi-static typical response for RO microstructure to the loading orientation, and normalized experimentally evaluated.

For the HO-90° samples, the material exhibits significant ductility, represented by a large increase of strain to failure (+55%) and the ultimate stress is divided by 4 compared to 0° samples. For this testing direction the overall behavior is mainly governed by the matrix properties. Conversely to the RO configuration, the HO presents an elastic anisotropy. Table 3 summarizes the averaged properties for the HO configuration tested at 0°, 45°, and 90°.

Based on the experimental findings, the anisotropy exhibited by the AC-SMC HO is clearly demonstrated compared to the RO configuration. As mentioned above, this anisotropy is due to the microstructure orientation induced by the specific filling mode during the thermo-compression process of HO configuration. In addition, the HO-0° response can be considered as an upper bound of the overall behavior of the AC-SMC composites, whereas the HO-90° response constitutes a lower bound.

Qualitative QS damage investigation. Post-mortem analyses were conducted on different tested samples. Firstly, the samples were radiographed using X-ray (Figures 11 and 12). Then the damage mechanisms taking place within the sample are investigated through SEM observations. The most significant results are presented in Figure 13.

On the radiographies of RO samples shown in Figure 11, a complex network of cracks is observed, which covers a substantial area of the ZoI. The network is composed of two kinds of cracks: on the one hand clustered and parallel cracks and on the other hand broader entangled ones. As their local orientation, proximity, and limited width suggest, the first ones are assumed to take place within the bundles.

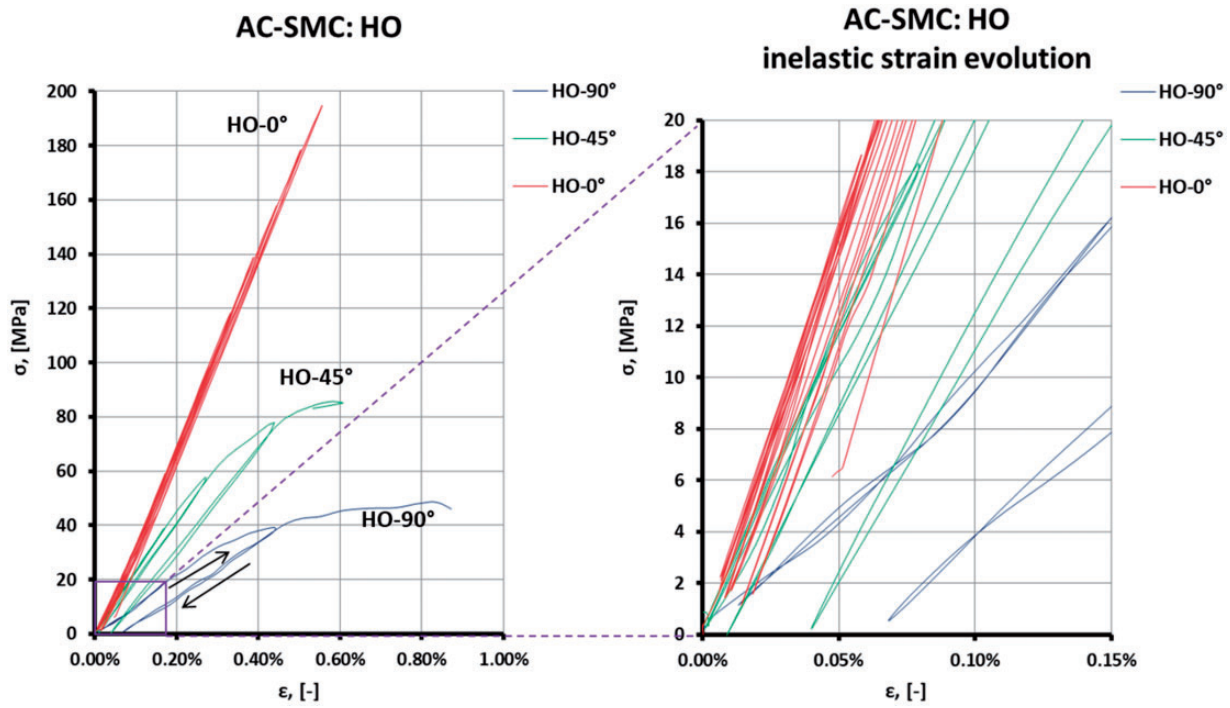

Figure 10. Quasi-static typical (σ, ϵ) response for HO microstructure with respect to the loading orientation and normalized experimentally evaluated.

Table 2. Mechanical properties experimentally determined for AC-SMC RO.

AC-SMC RO		0°	45°	90°
E	Avg. (GPa)	35.9	26.2	26.7
	CoV	9%	6%	16.6%
σ_{Iuts}	Avg. (MPa)	208	150	159
	CoV	17%	6.9%	15.1%
$\varepsilon^{I}_{f.}$	Avg. (%)	0.67	0.65	0.76
	CoV	23%	17.7%	15.8%

AC-SMC: advanced carbon-sheet molding compound; RO: randomly oriented.

Table 3. Mechanical properties experimentally determined for AC-SMC HO.

AC-SMC-HO		0°	45°	90°
E	Avg. (GPa)	39.4	23.5	13.5
	CoV	9.3%	10.2%	16%
σ_{uts}	Avg. (MPa)	180	90	55.4
	CoV	21.4%	10%	14%
ε^{I}_{f}	Avg. (%)	0.52	0.58	0.66
	CoV	55.7%	20.3%	22%

AC-SMC: advanced carbon-sheet molding compound; HO: highly oriented.

Contrarily, the second ones are presumed to happen at the scale of the bundle. If at 0° the whole region is affected by such network, the affected area and the network complexity decreases as the loading angle grows, leading to a less diffusive damage evolution.

Post-mortem radiographies of HO samples are shown in Figure 12. The samples loaded at 45° and 90° present a crack network similar to the RO samples subjected to the same loading conditions: the failure occurs along the MMFD in both cases. According to the microstructure of the HO samples, the cracks follow the reinforcement orientation. In the two radiographies of HO-00° there are less diffuse cracks of type 1 and cracks of type 2 are concentrated in a band of a single orientation (around 45° for HO-00° (1) and 90° for HO-00° (2) with respect to the longitudinal direction). Overall, in all configurations it is clear that two levels of damage are present: intra-bundle damage in the form of long and thin cracks and inter-bundle damage in the form of large, opened cracks that can lead to the failure of the specimen.

To further investigate, at a lower scale, where and how the damage mechanisms take place, the fracture area of post-mortem samples was observed using of SEM. The failure surface of an AC-SMC RO sample loaded at 0° is shown in Figure 13, with a focus on several areas of interest. Such analysis confirms the hypothesis of a two-scale damage pattern (intra and inter-bundle). Inter-bundle damage takes place in the

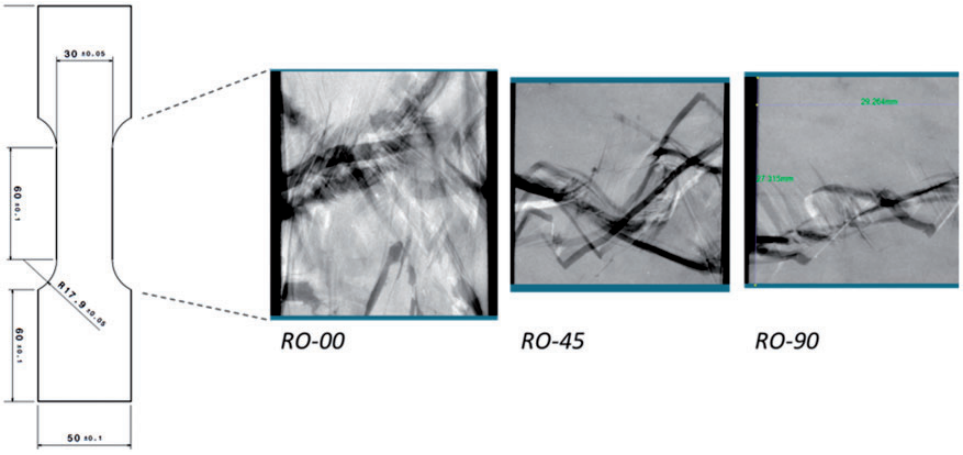

Figure 11. X-ray radiographies of broken RO samples loaded in different directions.
RO: randomly oriented.

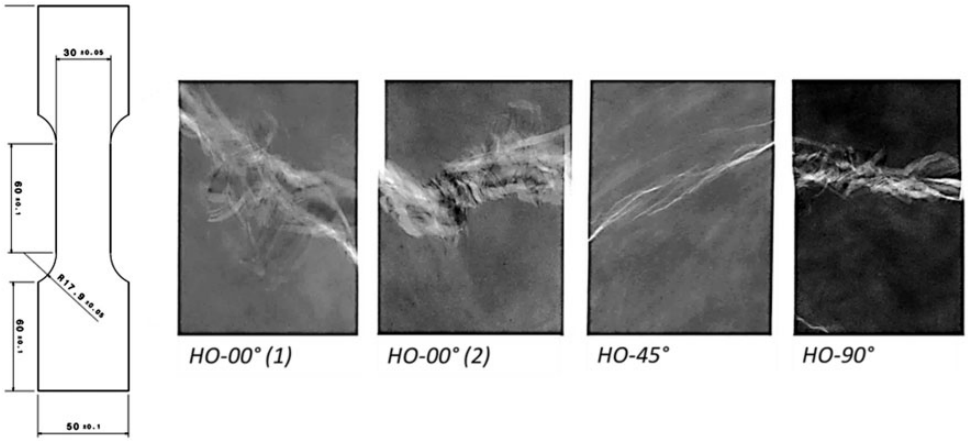

Figure 12. X-ray radiographies of broken HO samples loaded in different directions.
HO: highly oriented.

form of fiber pull-out and fiber debonding. Inside the bundle the damage is primarily characterized by matrix cracking in the areas where there is sufficient pure matrix volume.

The observation of the fracture surfaces by SEM also shows that bundles keep their integrity, the macro cracks of type two that leads to the final failure of the specimens occurs between the bundles.

Quantitative QS damage investigation. During the incremental QS loading-unloading tests, following the procedure presented in the section devoted to the description of the experimental methodology, the evolution of stiffness is monitored up to failure. The elastic modulus is evaluated for each unloading between 0.05% and 0.2% of the measured strain according to the standard ISO 527. Such evolution is presented in Figures 14 and 15 with respect to the loading orientation for each material configuration (HO and RO, respectively). All the results are normalized with respect to the original stiffness of each sample in the considered loading direction. For HO samples (Figure 14), it is observed that during the loading at 0°, the stiffness is constant up to failure. This indicates that the induced damage up to failure, if any, is organized in such a way that the stiffness in the loading direction is not affected.

As the loading angle shifts away from the MMFD, the stiffness degradation prior to failure increases, dropping down to 65% oriented at 90°. Those observations are consistent with the analogy with a UD composite, since for HO samples most of the bundles are oriented around the 0° direction.

Considering the RO samples, the stiffness degradation is shown in Figure 15 for the same loading conditions. While a similar trend is observed, i.e. the stiffness degradation increases with the angle of loading, the range of this degradation is limited from 6% at 00° and up to 17% at 90°. As discussed in the previous

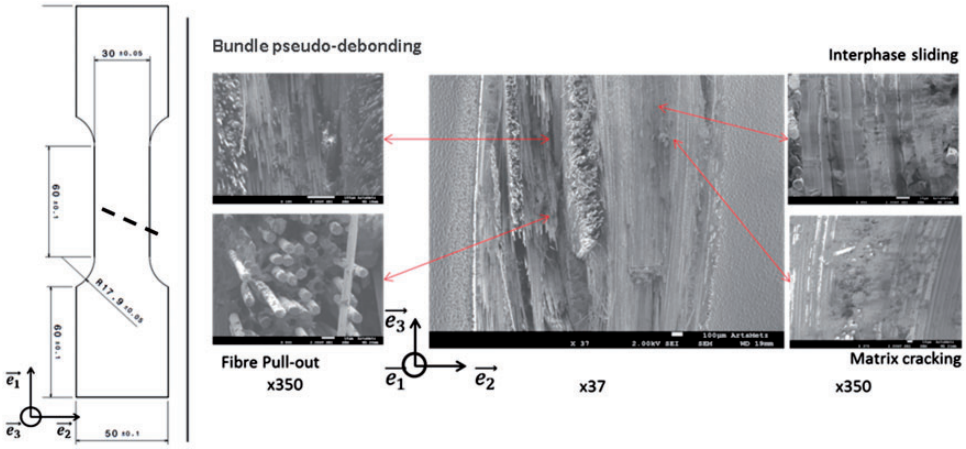

Figure 13. Qualitative damage investigation, SEM observation of the failure area (dashed line) of an AC-SMC RO sample at 00 °. AC-SMC: advanced carbon-sheet molding compound; RO: randomly oriented.

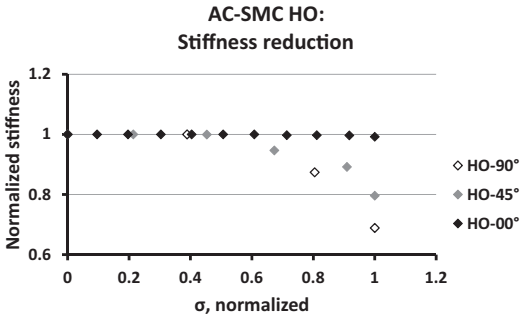

Figure 14. Stiffness evolution for AC-SMC HO configuration with respect to their respective loading stress for three different orientation of the loading 0 °, 45 °, 90 °.
AC-SMC: advanced carbon-sheet molding compound; HO: highly oriented.

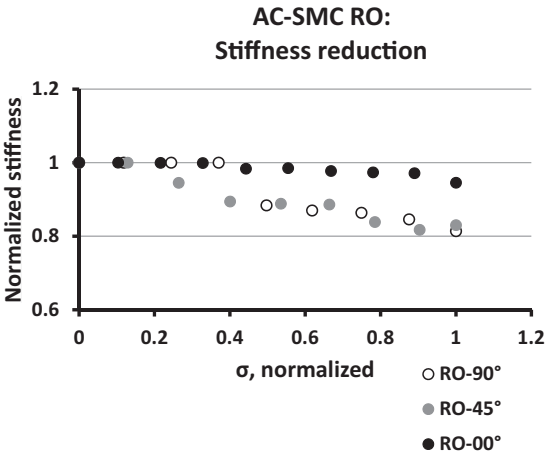

Figure 15. Stiffness evolution for AC-SMC RO configuration with respect to their respective stress and loading orientation.
AC-SMC: advanced carbon-sheet molding compound; RO: randomly oriented.

section, such results do not correspond to expected results coming from a pure random distribution of bundles. However, the overall mechanical responses of RO samples are clearly closer to the expected behavior of composites with a random distribution of the bundles compared to those obtained for HO samples. The critical stress for the onset of damage, relative to the ultimate stress of each sample, is globally lower for the RO samples than it is for the HO samples.

The stiffness reduction of the HO samples, and to some extent of the RO sample, can be analyzed following the results of micromechanical models that consider damage as a growth of ellipsoidal voids. Except towards the last cycles prior to failure, the crack network is mostly composed of thin intra-bundle cracks whose propagation occurs in a plane parallel to the bundle direction. At this scale, a bundle can be considered as a UD composite, composed of aligned carbon fibers embedded in a surrounding matrix.

Praud et al.[24] have considered the evolution of such long, thin crossing microcracks oriented in the transverse direction with respect to the direction of reinforcement in UD composites (the two small half-axis of the ellipsoid lies in a plane, which the normal direction is reinforcement). It is shown that in this case, the longitudinal stiffness is weakly impacted, while the in-plane shear and transverse modulus are significantly impacted with the appearance of such crossing microcracks. Since, especially in the HO configuration, bundles are mainly oriented in the MMFD direction (0°), the observed stiffness reduction is typical of the apparition of long, thin intra-bundle cracks.

Inelastic strain evolution. During the incremental QS loading-unloading tests, proceeding in the same manner as

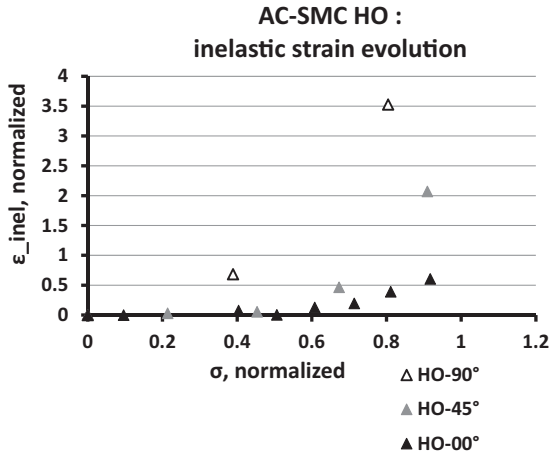

Figure 16. Inelastic strains evolution for AC-SMC RO configuration with respect to stress and loading orientation.
AC-SMC: advanced carbon-sheet molding compound;
RO: randomly oriented.

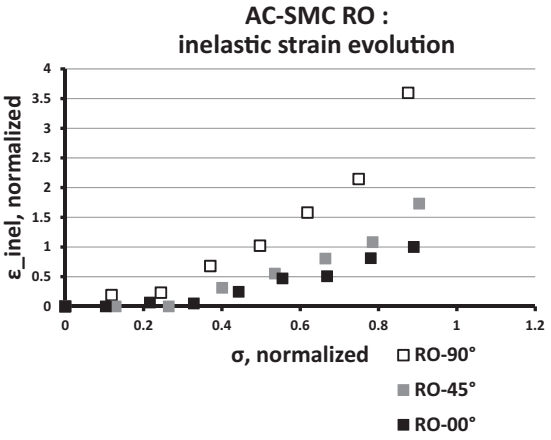

Figure 17. Inelastic strains evolution for AC-SMC RO configuration with respect to stress and loading orientation.
AC-SMC: advanced carbon-sheet molding compound;
RO: randomly oriented.

for the stiffness evolution, the inelastic strain evolution has been recorded and is shown in Figures 16 and 17. It is worth mentioning that, for the sake of visibility, the stress on the abscissa is normalized with respect to the ultimate stress in the considered direction.

The inelastic strain occurred during loading of HO specimen. The evolution of HO configuration (Figure 16) follows qualitatively the same evolution as observed for stiffness degradation: a limited evolution prior to failure at 0°, which is the signature of a brittle failure. In addition, for the loading cases at 45° and 90°, the level of inelastic strain reached indicates a ductile failure. Again, the global evolution of inelastic strain observed in HO specimen is comparable to what is generally observed for UD composites.

Considering the RO configuration (Figure 17), the same trend as for the stiffness degradation is also observed. Indeed, the development of inelastic strain starts at the same stress level as the onset of stiffness degradation, earlier than for the HO specimen. The evolution of inelastic strains, similarly to what has been observed for the stiffness degradation, do not correspond to the expected evolution of a composite reinforced with RO bundles. The evolution is not identical for all directions, and is more important when the angle deviates from the MMFD.

The analysis of the stiffness degradation and the inelastic strain evolution for both RO and HO specimens indicate that their respective evolution starts at the same load level, with a similar trend. This allows formulating the assumption that both mechanisms are coupled. As those inelastic strains remains limited (quasi-brittle failure) and their evolution follows the stiffness evolution such inelastic strains are considered to be induced by the damage. These experimental observations and conclusion are consistent with those made by Dano et al.[25]

Table 4. Advanced sheet molding compound (A-SMC) composition and constituents' weight content.[4,5]

Composition	Content (in weight ratio)
Vinyl-ester resin	24%
Glass fiber bundles	50%
Filler	24%
Additives	2%

Comparison with a SMC obtained with the same manufacturing process. The mechanical properties and the specific characteristics in relation with damage failure of the AC-SMC are compared with A-SMC materials studied by Shirinbayan et al.[4,5] The weight contents of A-SMC constituents are given in Table 4. Both materials are produced with the same vinyl-ester resin and thermo-compression process, both RO and HO configurations are obtained with the same method, and the process direction of the raw sheet coincides with the 0° orientation for both configurations. Their sole differences are the nature of the reinforcement and the thermo-compression parameters. The A-SMC[4,5] material is reinforced by bundles of glass fibers and fillers, whereas AC-SMC material is only reinforced by bundles consisting of carbon fibers. In contrast to AC-SMC, the A-SMC configurations are thermos-compressed under a pressure of 135 bar, at the same temperature (150°C), however with a shorter process time: 90 s.

From the previous experimental observations and analysis, it can be concluded that the AC-SMC RO

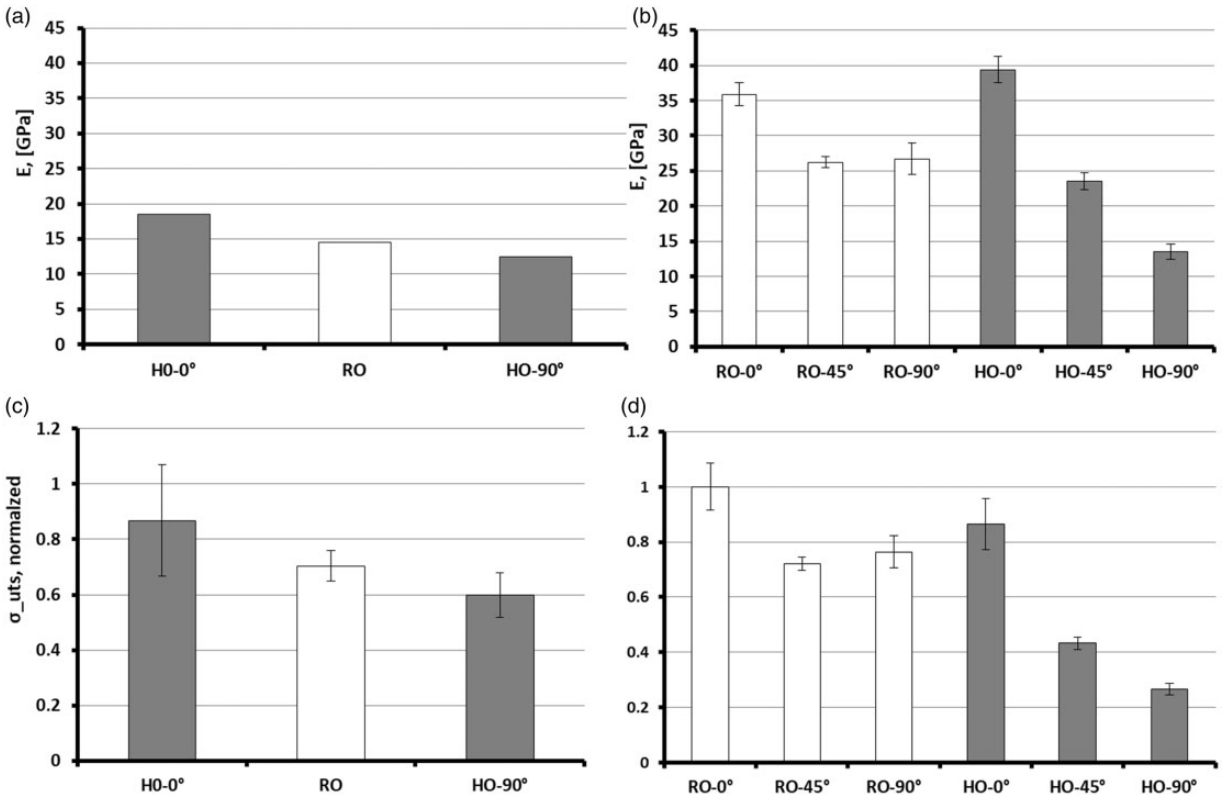

Figure 18. Comparison between A-SMC and AC-SMC elastic moduli of the (a) A-SMC[4] and (b) AC-SMC, and ultimate tensile strength (c) A-SMC results normalized with respect to AC-SMC RO 0°, (d) AC-SMC.
A-SMC: advanced sheet molding compound; AC-SMC: advanced carbon-sheet molding compound.

do not exhibit an in-plane isotropic behavior, leading to two assumptions: either the RO molding process induces a main direction or the observed behavior of the RO configuration results from the raw sheet manufacturing process. In Figure 18, the elastic moduli and normalized ultimate stress of respectively A-SMC (Figure 18(a) and (c)) and AC-SMC (Figure 18(b) and (d)) samples are presented with respect to loading angles and configuration. It is worth mentioning that the information about the A-SMC (Figure 18(a) and (c)) are extracted from Shirinbayan et al.[5] All ultimate stress values (Figure 18(c) and (d)) are normalized with respect to one of the AC-SMC RO at 0°. Note that in the A-SMC case, since the RO configuration exhibits an in-plane isotropic overall response according to Shirinbayan et al.,[4,5] results for 00° and 90° (Figure 18(a)) are gathered. In fact, it has been established that both the elastic modulus and the normalized ultimate stress of the configuration A-SMC RO does not depend on orientation.[4,5]

Firstly, the comparison of the A-SMC and AC-SMC respective stiffness (Figure 18(a) and (b)) highlight the higher elastic modulus of the AC-SMC in both configurations for every considered direction. It is particularly noticeable that in the case of the HO configuration: the AC-SMC stiffness in the MMFD is twice the one of the A-SMC. The ratio of the stiffness for the configuration HO in the 0° and 90° is also higher in the AC-SMC compared to that in the A-SMC ($R^{HO}_{0°-90° A-SMC} = 1,48 < 2,92 = R^{HO}_{0°-90° AC-SMC}$).

Secondly, the comparison of the A-SMC and AC-SMC normalized ultimate stress (Figure 18(c) and (d)) highlights the following observations. On one hand, the ultimate stress on RO samples is higher for the AC-SMC regardless of the orientation; however, on the other hand, the ultimate stress of AC-SMC HO strongly depends on the orientation. Specifically, the ultimate stress at 90° is significantly lower for the AC-SMC compared to the A-SMC one. Proceeding in the same manner as for the elastic moduli, the ratio of the ultimate stress in the HO configuration between 0° and 90° presents a higher level of anisotropy for the AC-SMC ($R^{HO}_{0°-90° A-SMC} = 1,47 < 3,22 = R^{HO}_{0°-90° AC-SMC}$).

Based on the experimental findings comparing the A-SMC and AC-SMC in terms of their respective elastic moduli and ultimate stress, it comes out that for a same fiber content the AC-SMC is suitable for structural applications where a high stiffness is required.

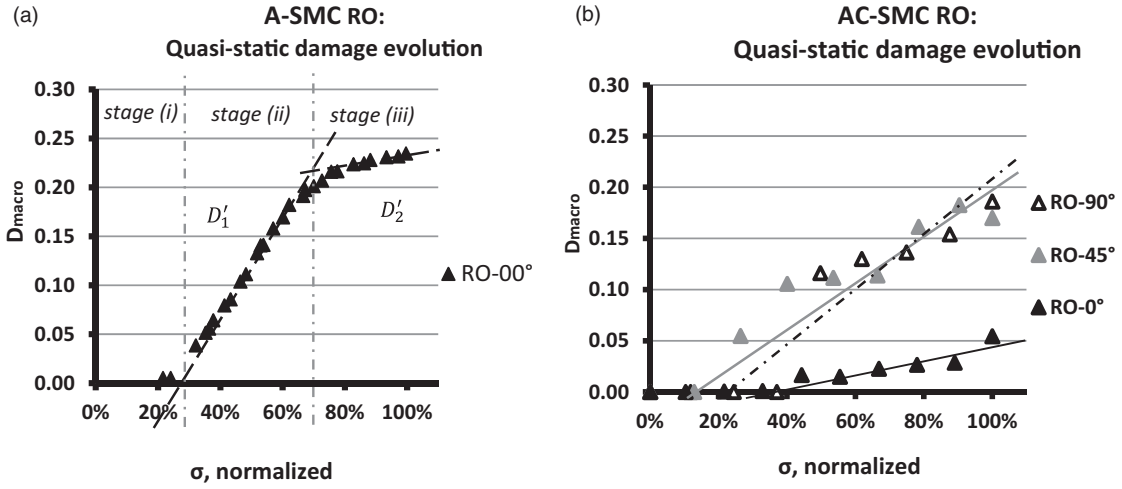

Figure 19. Damage evolution under quasi-static for (a) A-SMC RO[4] and (b) AC-SMC.
A-SMC: advanced sheet molding compound; AC-SMC: advanced carbon-sheet molding compound; RO: randomly oriented.

The A-SMC composites are more appropriate than the AC-SMC for applications where a high strength-to-cost ratio is required.

Besides the comparison between A-SMC and AC-SMC composites in terms of ultimate stresses (Figure 18(a) and (b)), the macroscopic damage evolutions are analyzed and compared for the RO configurations for both SMCs Figure 19(a) and (b). On the one hand, the damage evolution of A-SMC RO exhibits three stages (Figure 19(a)): (1) the damage initiation, which occurs at 25% of the ultimate tensile stress. It is followed by (2) a rapid evolution at a relatively high quasi-constant rate (the slope $\frac{\Delta D}{\Delta \sigma} = D_1^{'}$). For this second stage, the damage accumulation reaches $D_{\text{macro}} = 0.2$ for an applied stress up to 73% of σ_{uts}. The third and ultimate damage stage (3) is characterized by a reduced damage rate ($D_2' < D_1'$). It corresponds to the damage saturation prior to the specimen's failure. During this saturation, the damage reaches a critical level of 0.25 before failure. On the other hand, as shown in Figure 19(b), the AC-SMC RO exhibits only a two-step damage evolution: (1) the initiation, which depends on the sample orientation, and (2) the accumulation stage. Conversely to the A-SMC, non-saturation stage has been observed preceding the specimen failure. In addition, the maximal damage level (critical level) reached prior to the failure depends on the sample's orientation. In Figure 19(b), one can notice that the damage evolution and the critical damage levels depend on the sample orientation. For the 0° specimen, the critical macroscopic damage level is about 0.06, whereas for 45° and 90°, the maximal level of damage prior to failure is respectively equal to 0.17 and 0.18. Furthermore, for 45 and 90°, the damage initiation and evolution stages are comparable, whereas for AC-SMC RO 0°, the initiation of the damage is delayed (33% of σ_{uts}) and its evolution is clearly reduced. Indeed, due to the fact that the damage evolution is comparable between 45° and 90°, their respective σ_{uts} are of the same order of magnitude as mentioned previously. Lastly, it is worth noticing that the damage threshold in AC-SMC RO depends on the sample orientation.

The comparison highlights three main conclusions: (1) the thermo-compression in the RO configuration results in a transversally isotropic response of A-SMC composite and an in-plane anisotropic overall response for the AC-SMC composite. (2) The difference between the HO and RO configurations (effect of the process induced orientation) is more pronounced for the AC-SMC than for the A-SMC samples. (3) This difference affects drastically the damage evolution and the ultimate strength, especially for AC-SMC at 45° and 90°.

Fatigue test results

To characterize the fatigue response of AC-SMC composites, cyclic tensile tests have been performed for various orientations of the RO and HO samples.

Evolution of the mechanical response of RO samples oriented at 0°. AC-SMC RO samples have been loaded at 80% of σ_{uts} at a frequency of 10 Hz with a load ratio of 0.1 up to failure. Under those loading conditions, considering a batch of seven samples, the fatigue life N_{50} pertaining to the median fatigue life is 11,832 cycles. This value corresponds to the minimal fatigue life of at least 50% of the tested specimen of the considered batch, under the same loading conditions. Specifically, one specimen of the considered bath has been selected that failed at 4591 cycles, which is the lowest life from this batch. The analysis of the evolution of the

mechanical response is therefore considered to be conservative compared to the other specimens of the batch. The evolutions of the mechanical response at different cycles have been recorded and are shown in Figure 20. The evolution of three characteristics is analyzed: the shape of the hysteresis loop (Figure 20), the macroscopic damage $D(N) = 1 - \frac{E(N)}{E_0}$ (Figure 21(a)), and the permanent strain (Figure 21(b)).

The shape of the hysteresis loop (Figure 20) stays constant throughout the number of cycles, which indicates that the mechanical dissipation is not evolving significantly, even if only a careful analysis of the thermal field is required to properly conclude on the fraction of mechanical work that is dissipated into heat.

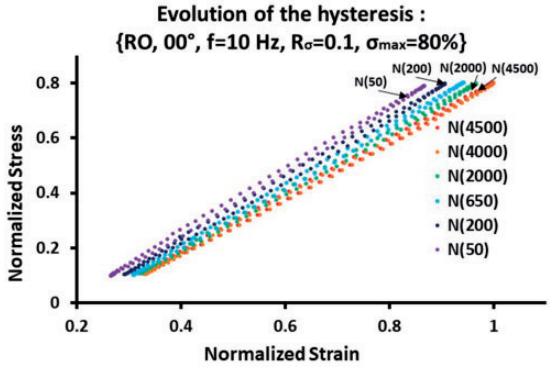

Figure 20. Evolution of the hysteresis with respect to cycles of an RO ° sample loaded under ($f = 10$ Hz, $R\sigma = 0.1$, $\sigma_{max} = 80\%$). RO: randomly oriented.

The evolution of macroscopic damage with respect to the number of cycles is shown in Figure 21(a) for the AC-SMC RO samples oriented in the MMFD for an applied stress at 80% of σ_uts. The fatigue macroscopic damage exhibits a non-linear evolution: the rate of damage with respect to the number of cycles is the highest at the beginning, and drastically reduces around 35 cycles. A progressive evolution is observed afterwards, while the rate continuously decreases, as it is often noticed in the fatigue response of glass or carbon fibers reinforced SMC composites.[25,26] Actually, after the cycle 4000 and prior the cycle to failure, no damage evolution has been noticed. Final failure happens with a level of macroscopic damage that is much higher than the one observed during QS tests. This indicates that the stiffness reduction is not the appropriate characteristic to monitor, and it is unable to predict the final failure of this material. Damage mechanisms should be observed and tracked at lower scales to identify the damage modes that eventually lead to failure. In Figure 21(b), the evolution of macroscopic permanent strain (normalized with respect to the ultimate permanent strain previously evaluated) is presented. A curve describing evolution of the permanent strain would present an exponential type shape in the semi log-scale graph. Actually, it is observed that the permanent strain evolves linearly with the number of cycles. At $N = 4000$ cycles, the permanent strain reaches eight times that established in QS tests, making this feature as inappropriate to monitor to predict final failure as macroscopic damage.

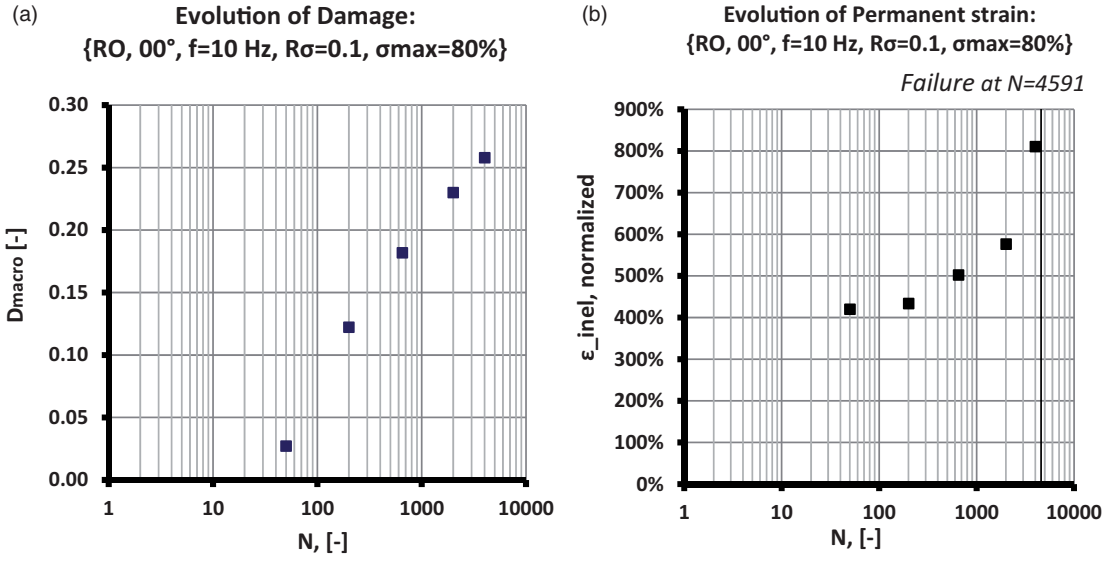

Figure 21. Evolution of (a) damage and (b) permanent strain, for a RO-00 ° sample loaded under ($f = 10$ Hz, $R_\sigma = 0.1$, $\sigma_{max} = 80\%$). RO: randomly oriented.

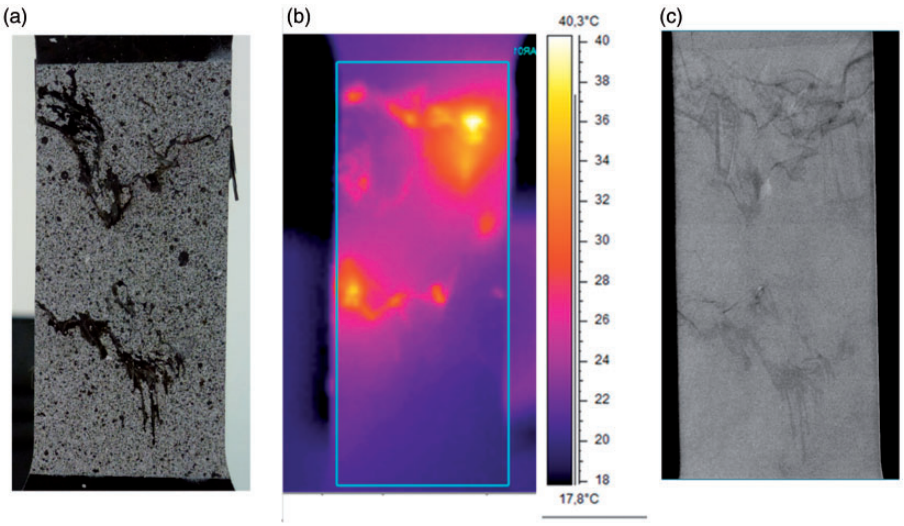

Figure 22. Qualitative observations of the sample ZoI: (a) post-mortem photo, (b) thermal field computed at failure from the IR-CCD, and (c) post-mortem X-ray shot.
ZoI: Zone of Interest.

Following each fatigue test, a qualitative post-mortem investigation is conducted on the samples. This systematic analysis is composed of an optical picture of the sample surface, a map of the temperature at the surface computed from infra-red picture and X-ray radiography. Those results are presented in Figure 22 for the sample loaded up to failure. Two complex cracks networks within the ZoI can be observed in the optical picture (Figure 22(a)). The X-ray shot further unveils the complexity of the cracks networks, since those cracks are not superposed throughout the thickness of the specimen (Figure 22(c)). As observed in the post-mortem analysis of samples after a QS tensile loading up to failure, two types of cracks compose the networks: cracks thin and parallel, as well as broader and entangled ones. The thermal field computed from the last infra-red picture prior to failure (Figure 22(b)) highlights the strong heterogeneous temperature field at the surface of the specimen. Temperature varies from ambient temperature (20°C) to a maximum of 40.3°C. In area where a crack network is observed through radiography, the temperature is significantly higher. However, the highest temperature is not measured close to the macro-cracks that have appeared on the surface of observation. A hot zone in the upper right area of the ZoI corresponds to the high density of cracks that can be seen with X-ray radiographies, which highlights the importance of damage through the thickness of the sample that might have not affected the surface.

Effect of microstructure and loading orientation on the evolution of fatigue damage. The importance of the microstructure (RO versus HO samples) is investigated based on a fatigue experimental characterization test campaign performed at a frequency of 10 Hz and with a load ratio of 0.1. Samples were loaded at different levels of maximum stress that have been normalized with respect to the ultimate stress of the RO sample loaded in the 0° direction. The obtained normalized S-N curves are presented in Figure 23(a) for the RO samples loaded in the 0°, 45°, and 90° direction and in Figure 24 for RO and HO samples loaded in the 0° direction. The samples that survived 10^6 cycles are identified with an arrow. It can be noted that the fatigue life of samples loaded at a maximum stress value of 0.6 and below (relative to the σ_{uts} RO sample loaded at 0°) is very scattered, with orders of magnitudes that can reach four decades. Figure 23(b) shows reduced S-N curves considering a median fatigue life N_{50}. Overall, for all the considered orientation, the median fatigue life (N_{50}) increases when decreasing the maximum stress. In Figure 23(c) the standard deviation (variability) of the fatigue life of RO samples loaded in the 0°, 45°, 90° and HO samples loaded in the 0° direction is plotted with respect to the applied maximum stress. Note that the variability has been estimated considering that the fatigue life limit corresponds to 10^6 cycles. The variability increases by decreasing the maximal stress level. This trend is also noticed for the 0°, 45°, and 90° orientations.

The comparison between the S-N curves for RO and HO samples (loaded at 0°) is shown in Figure 24(a). Figure 24(b) shows the fatigue life (N_{50}) with respect to the maximum stress plotted for both previous samples. At all stress levels, for either RO or HO samples, the results in terms of number of cycles up to failure is also very scattered, with orders of magnitudes that can reach four decades. Note that the variability at high

maximum stress levels is higher for HO samples than the one observed for the RO samples (Figure 23(c)).

To sum up, the observations realized on the orientation effect under tensile QS loading are confirmed in tension–tension cyclic loading. Concerning the RO configuration, the differences in terms of ultimate stress feed through to a difference in terms of fatigue life. The spread of the result is aggravated due to the dispersive nature of cyclic testing and no meaningful difference could be made between the three loading angles. Concerning the HO orientation, 00° is the sole loading orientation tested. The results display a binary behavior: below a given threshold no failure was observed before 10^6 cycles, adversely over it the results covert the full span of the test. The nearer the maximal loading stress is to the threshold, the more frequently samples survive 10^6 cycles.

Load ratio effect. S-N curves, normalized with respect to the ultimate stress of the RO sample loaded in the 0°

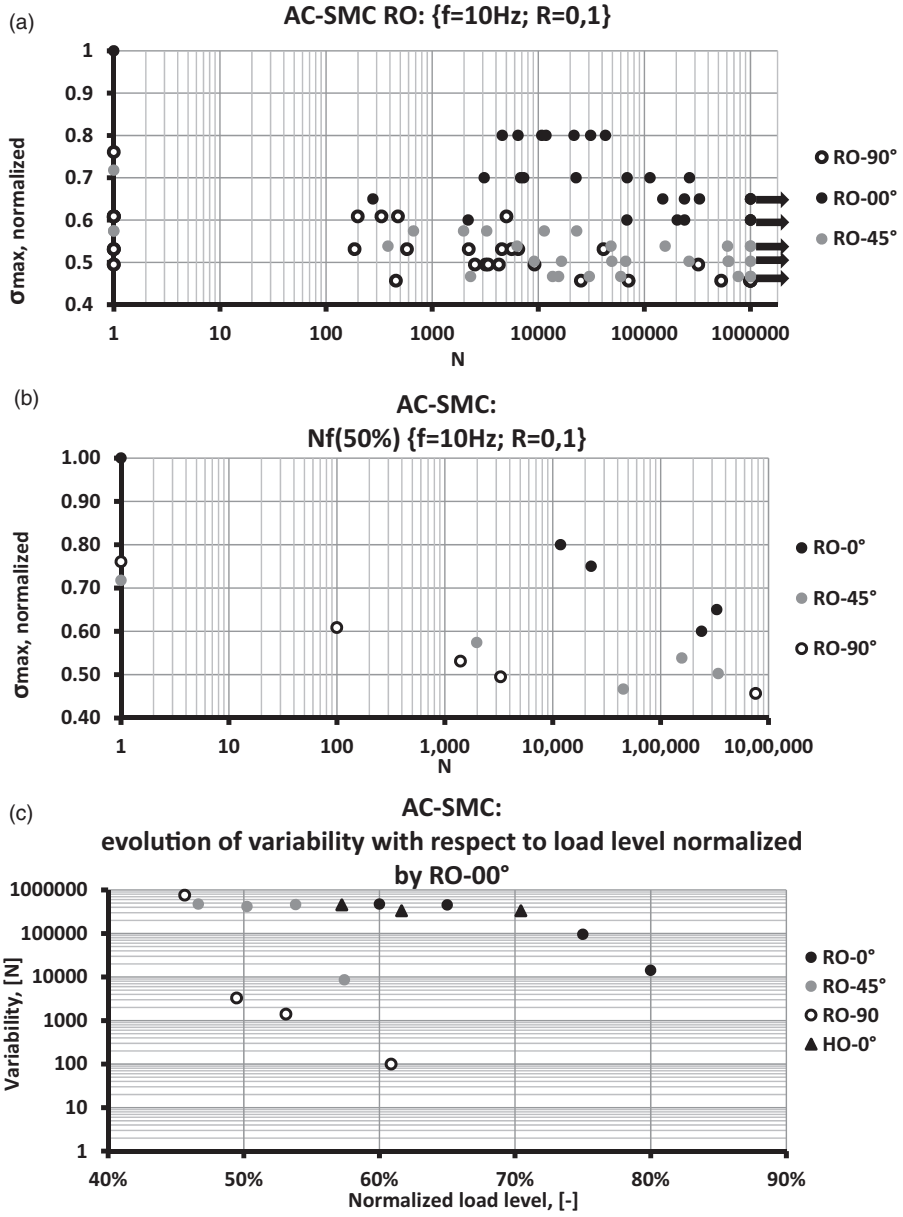

Figure 23. Fatigue results obtained on the AC-SMC RO normalized with respect to RO-00° S-N at a frequency of 10 Hz and a load ratio of 0.1, (a) S-N curve, (b) S-N at Nf (50%), and (c) evolution of measured variability at each load level for the three considered orientation for RO and only at 00° for HO.
AC-SMC: advanced carbon-sheet molding compound; RO: randomly oriented; HO: highly oriented.

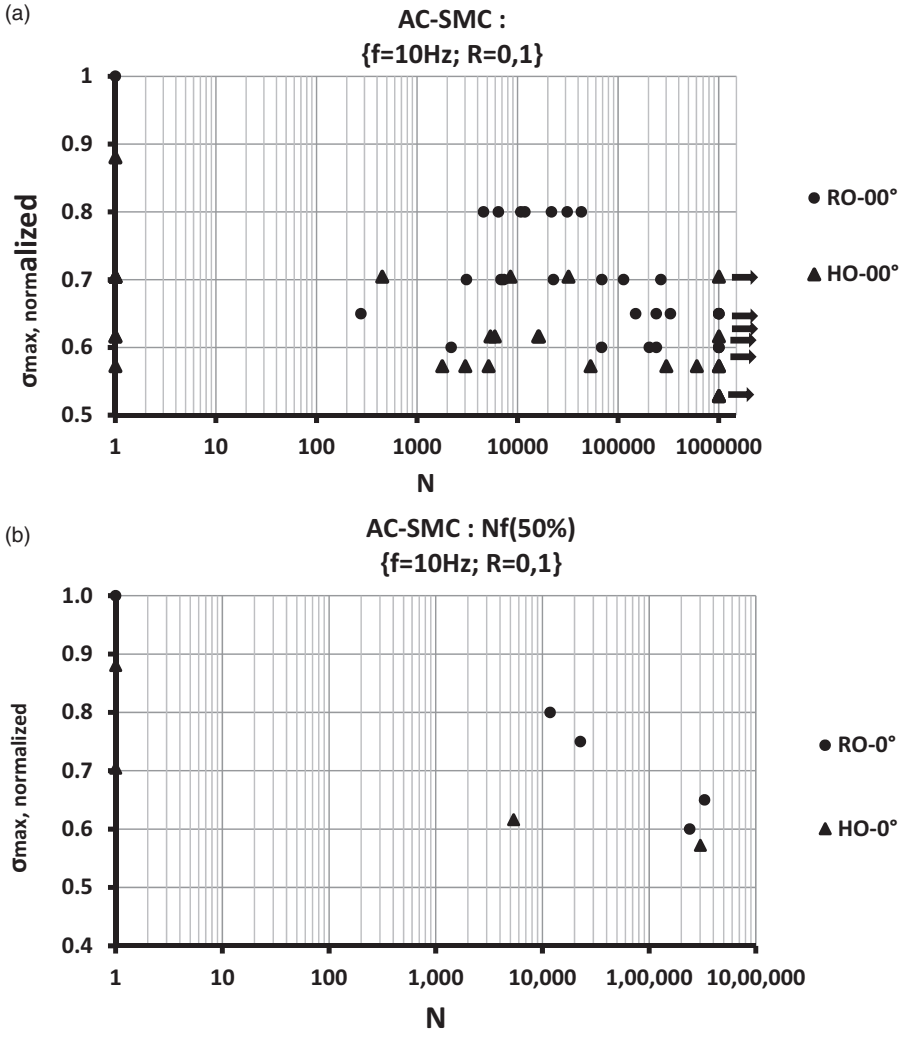

Figure 24. AC-SMC RO and HO at a frequency of 10 Hz and a load ratio of 0.1, (a) S-N curves normalized with respect to RO-00 °and (b) results for Nf (50%) normalized with respect to RO-00 °.
AC-SMC: advanced carbon-sheet molding compound; RO: randomly oriented; HO: highly oriented.

direction, obtained at a load ratio of 0.1 and 0.4 for one load level in the case of RO samples are presented in Figure 25(a), for samples oriented at 0° and 90°, and Figure 25(b), for samples oriented at 45°. Considering the specimen loaded in the 45° direction, three load levels have been tested (75%, 70%, and 60% of $\sigma_{\text{uts}}(\text{RO} - 45^\circ)$). For the following comparison between several orientations of sample, all the values have been normalized with respect to $\sigma_{\text{uts}}(\text{RO} - 00^\circ)$.

At 0°, we observe no significant influence for both the fatigue life and its variability. At a loading orientation of 90°, a notable increase of the fatigue life is observed for a ratio of 0.4 compared to the ratio of 0.1. For the 45° loading direction, if at a maximal loading stress of $0.47\sigma_{uts}(RO - 00^\circ)$ no major difference is observed, at the other two maximal loading stresses 57% and 54% of $\sigma_{uts}(RO - 00^\circ)$, we observe a global increase of the fatigue life with a load ratio of 0.4. Furthermore, we observed a higher number of samples surviving 10^6 cycles at $\sigma_{max,norm.} = 0.50\sigma_{uts}(RO - 00^\circ)$ with respect to $\sigma_{max,norm.} = 0.57\sigma_{uts}(RO - 00^\circ)$. However, there is still no meaningful impact on the variability.

To summarize, similar tendencies are observed on the orientation effect under tensile QS loading and tension–tension fatigue loading converge towards the same tendencies: (1) Concerning the RO configuration, the evolution of level of ultimate stress with the loading angle is correlated with evolution of the fatigue life with the loading angle; (2) While it is commonly observed that a higher load increases the fatigue life, such observation is not clear regarding the RO samples (note that only load ratio of 0.1 and 0.4 have been tested) and depends on the loading orientation and

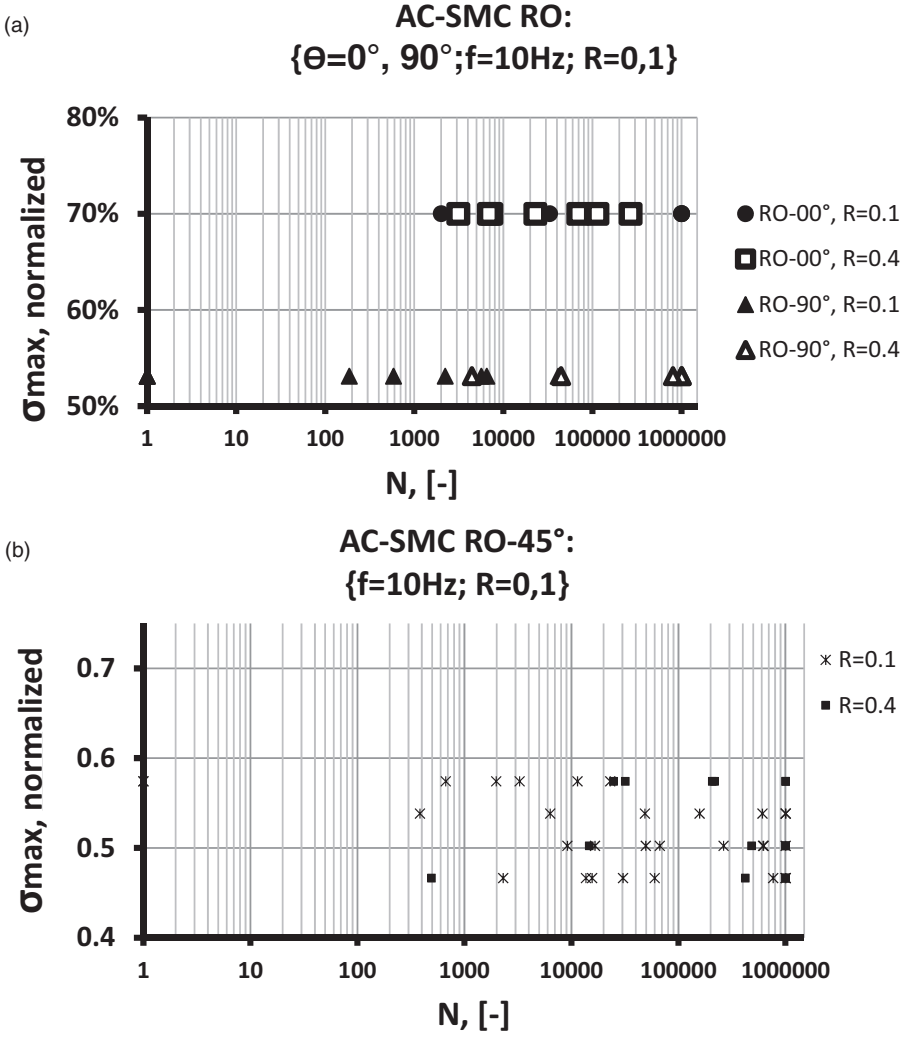

Figure 25. Normalized S-N curves for RO-00 °, RO-45 °, RO-90 ° at 10 Hz with a load ratio of 0.1 and 0.4, (a) results for RO-0 ° and 90 °, (b) results for RO-45 °.
RO: randomly oriented.

maximum stress. A more in-depth study of the effect of load ratio on the evolution of damage should be pursued to be able to draw noticeable conclusions.

Comparison of the fatigue response of AC-SMC and A-SMC. Similarly, with the analysis of QS experimental tests, the fatigue experimental characterization presented here is compared with the results obtained by Shirinbayan et al.[4] on the A-SMC obtained with the same manufacturing process. In Figure 26, the results of the tension–tension stress-controlled cyclic tests performed on the A-SMC with a load ratio of 0.1, a frequency of 10 Hz for RO, HO-00°, and HO-90° samples are presented from the results provided by Shirinbayan et al.[5] The obtained S-N curves are normalized with respect to RO ultimate stress. If it is not possible to determine the variability of the fatigue life, a clear Wöhler curve can be observed obtained from the cyclic test results, suggesting a small scattering of the fatigue life. Those curves display a typical bilinear form for every tested orientation and configuration RO and HO-90° samples exhibit a similar fatigue life. Considering the A-SMC RO, between an applied stress of 0.44 and $0.39\sigma_{uts}(RO)$, the fatigue life jumps from $50,000$ to 10^6 cycles.

As for the AC-SMC, the behavior under tension–tension fatigue loading is strongly influenced by the configuration of the composite material. If the dispersive nature of the AC-SMC restricts the determination of a Wöhler curve with a good confidence, such difficulty does not exist for the A-SMC. In order to reliably draw those fatigue curves for the AC-SMC, further

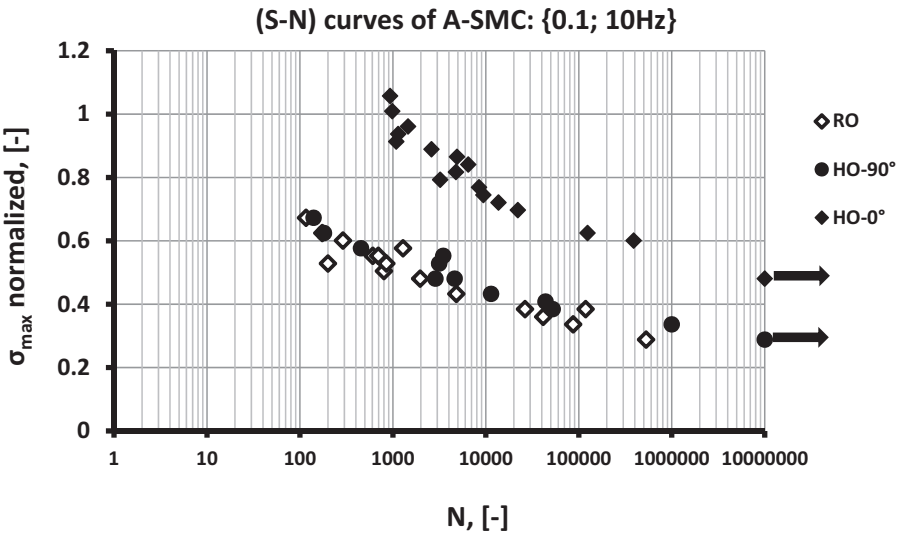

Figure 26. S-N curves of A-SMC, normalized in stress with respect to the ultimate stress of AC-SMC RO-0°, obtained with a load ratio of 0.1 and frequency of 10Hz, for HO-00° RO and HO-90° samples from Shirinbayan et al.[5]
AC-SMC: advanced carbon-sheet molding compound; RO: randomly oriented; HO: highly oriented.

testing is required as the actual number of tested samples is too low to conduct a reliable statistical analysis on the data.

Conclusion

In this paper, the characterization of the mechanical behavior of a new class of SMC reinforced carbon fiber bundles (AC-SMC) has been carried out through QS tensile tests with incremental loading/unloading loops and tension–tension load-controlled fatigue tests. The effect of the anisotropy induced by the thermo-compression process has been investigated through the comparative study of two configurations of this composite material: RO and HO. For both configurations, specimens were cut and tested along three directions (0°, 45°, and 90°). For QS tests, the influence of the process-induced orientation is studied in terms of ultimate strength, elastic modulus, and macroscopic damage corresponding to the stiffness reduction. With regard to fatigue tests, the effect of specimen orientation is analyzed in terms of S-N curves and macroscopic damage evolving with respect to the number of cycles. The obtained experimental results have been compared with those obtained on an equivalent SMC composite reinforced by glass fiber bundles (A-SMC). The following concluding remarks are drawn from these studies:

- Both configurations of AC-SMC exhibit a quasi-brittle in-plane anisotropic response. Especially for the RO configuration, this was a surprising result at a first glance, since one could expect an in-plane isotropic behavior, according to the established knowledge from the A-SMC composites. This non-conventional finding is associated with the manufacturing process-induced microstructure specific for AC-SMC.
- The microscopic investigations using post-mortem SEM and X-rays radiographies show that the damage modes occur as microcracks at two levels (inter-bundles and intra-bundles) and they depend on the sample orientation. The analysis of the macroscopic damage evolution for HO AC-SMC configuration reveals that samples in the MMFD direction (0°) exhibit very limited stiffness degradation whereas for other tested samples orientations the damage reaches respectively 0.2 and 0.32 for 45° and 90°. For RO AC-SMC small stiffness reduction prior to failure (6%) is observed in the MMFD direction, while similar critical levels (approximately 0.18) and kinetics are noticed for samples at 45° and 90°. In addition, the macroscopic damage evolution exhibits an evolution on two-stages (initiation and propagation) and no saturation was observed prior to the samples' failure, conversely to the damage evolution observed on A-SMC RO.
- In terms of ultimate stress, the difference between the HO and RO is more pronounced for the AC-SMC samples than for the A-SMC samples. This difference is amplified especially for AC-SMC at 45° and 90°.
- For the fatigue tests, the experimental results based on S-N curves analysis demonstrate that, with respect to the loading angle, the evolution of fatigue life of AC-SMC RO configuration exhibits the same

trend as the ultimate stress. A higher load ratio might increase the fatigue life of RO samples, though this is not observed in all situations and depends on the loading orientation and maximum stress. For the AC-SMC HO in the MMFD, the fatigue behavior has a similar trend and brittleness as that generally observed for a carbon fiber UD composite.
- The macroscopic damage of AC-SMC RO under fatigue loading shows a two-stages evolution similar to that observed for QS loading. In addition, the damage modes caused by fatigue in RO samples were also similar with those appearing under QS conditions.

This study highlights the key points differentiating the two types of SMC (carbon and glass) with chopped reinforcement. The degree of anisotropy was more pronounced for AC-SMC, due to the high dependency of the behavior on the manufacturing process-induced orientation. Furthermore, the damage evolutions of the two types of SMCs have displayed different kinetics, notably for the saturation stage which was not observed for the AC-SMC composite. These findings may guide the formulation of specific micromechanical modelling for these two types of composites, which should necessarily integrate the highlighted differences.

Acknowledgements

This paper is part of the COPERSIM project managed by IRT Jules Verne (French Institute in Research and Technology in Advanced Manufacturing Technologies for Composite, Metallic and Hybrid Structures). The authors wish to associate the industrial and academic partners of this project; respectively, Arts et Métiers ParisTech, Solvay, Plastic Omnium, PSA, and Renault.

Declaration of Conflicting Interests

The author(s) declared no potential conflicts of interest with respect to the research, authorship, and/or publication of this article.

Funding

The author(s) received no financial support for the research, authorship, and/or publication of this article.

ORCID iD

F Meraghni http://orcid.org/0000-0002-5043-8700

References

1. Jendli Z, Meraghni F, Fitoussi J, et al. Multi-scales modelling of dynamic behaviour for discontinuous fibre SMC composites. *Compos Sci Technol* 2009; 69: 97–103.
2. Oldenbo M, Fernberg SP and Berglund LA. Mechanical behaviour of SMC composites with toughening and low density additives. *Compos A Appl Sci Manuf* 2003; 34: 875–885.
3. Le T-H, Dumont PJJ, Orgéas L, et al. X-ray phase contrast microtomography for the analysis of the fibrous microstructure of SMC composites. *Compos Part A Appl Sci Manuf* 2008; 39: 91–103.
4. Shirinbayan M, Fitoussi J, Meraghni F, et al. High strain rate visco-damageable behavior of advanced sheet molding compound (A-SMC) under tension. *Compos Part B Eng* 2015; 82: 30–41.
5. Shirinbayan M, Fitoussi J, Meraghni F, et al. Coupled effect of loading frequency and amplitude on the fatigue behavior of advanced sheet molding compound (A-SMC). *J Reinf Plast Compos* 2017; 36: 271–282.
6. Palmer J, Savage L, Ghita OR, et al. Sheet moulding compound (SMC) from carbon fibre recyclate. *Compos A Appl Sci Manuf* 2010; 41: 1232–1237.
7. Odenberger PT, Andersson HM and Lundström TS. Experimental flow-front visualisation in compression moulding of SMC. *Compos A Appl Sci Manuf* 2004; 35: 1125–34.
8. Ferré Sentis D, Orgéas L, Dumont PJJ, et al. 3D in situ observations of the compressibility and pore transport in Sheet Moulding Compounds during the early stages of compression moulding. *Compos A Appl Sci Manuf* 2017; 92: 51–61.
9. Shirinbayan M, Fitoussi J, Abbasnezhad N, et al. Mechanical characterization of a low density sheet molding compound (LD-SMC): multi-scale damage analysis and strain rate effect. *Compos B Eng* 2017; 131: 8–20.
10. Bruderick M, Denton D, Shinedling M, et al. Applications of carbon fiber smc for the Dodge Viper. In: *Proceedings of the second S.P.E. automotive composites conference exhibition*, 2012. Retrieved from http://www.quantumcomposites.com/pdf/papers/Viper-SPE-Paper.pdf.
11. Evans AD, Qian CC, Turner TA, et al. Flow characteristics of carbon fibre moulding compounds. *Compos A Appl Sci Manuf* 2016; 90: 1–12.
12. Zaiß M, Jank MH, Netzelmann U, et al. Use of thermography and ultrasound for the quality control of SMC lightweight material reinforced by carbon fiber tapes. *Procedia CIRP*. 2017; 62: 33–38. DOI: 10.1016/j.procir.2016.06.039.
13. Denton DL. Mechanical properties characterization of an SMC-R50 Composite. *SAE Transactions* 1979; 88: 2283–2294. Retrieved from https://www.jstor.org/stable/44699057.
14. Wang SS and Chim ES-M. Fatigue damage and degradation in random short-fiber SMC composite. *J Compos Mater* 1983; 17: 114–134.
15. Hour K-Y and Sehitoglu H. Damage development in a short fiber reinforced composite. *J Compos Mater* 1993; 27: 782–805.
16. Trauth A, Pinter P and Weidenmann K. Investigation of quasi-static and dynamic material properties of a structural sheet molding compound combined with acoustic emission damage analysis. *J Compos Sci* 2017; 1: 18.

17. Mortazavian S and Fatemi A. Fatigue behavior and modeling of short fiber reinforced polymer composites: a literature review. *Int J Fatigue* 2015; 70: 297–321.
18. Guster C, Pinter G, Mösenbacher A, et al. Evaluation of a simulation process for fatigue life calculation of short fibre reinforced plastic components. *Procedia Eng* 2011; 10: 2104–2109.
19. Ogi K, Kim JW, Ono K, et al. Impact damage and residual tensile strength of a CF-SMC composite. *Adv Compos Mater* 2013; 22: 29–47.
20. Ogi K and Yamanouchi M. Temperature dependence of flexural strength of a CF-SMC composite. *Appl Compos Mater* 2011; 18: 397–408.
21. Trauth A, Bondy M, Weidenmann KA, et al. Mechanical properties and damage evolution of a structural sheet molding compound based on a novel two step curing resin system. *Mater Des* 2018; 143: 224–237.
22. Shirinbayan M. Étude du comportement mécanique et de l'endommagement de divers matériaux composites smc soumis à des chargements de type dynamique, fatigue et dynamique post-fatigue. PhD Thesis (in French). Retrieved from https://pastel.archives-ouvertes.fr/tel-01553663/document.
23. Brunbauer J and Pinter G. Effects of mean stress and fibre volume content on the fatigue-induced damage mechanisms in CFRP. *Int J Fatigue* 2015; 75: 28–38.
24. Praud F, Chatzigeorgiou G, Chemisky Y, et al. Hybrid micromechanical-phenomenological modelling of anisotropic damage and anelasticity induced by micro-cracks in unidirectional composites. *Compos Struct* 2017; 182: 223–236.
25. Dano M-L, Gendron G, Maillette F, et al. Experimental characterization of damage in random short glass fiber reinforced composites. *J Thermoplast Compos Mater* 2006; 19: 79–96.
26. Brunbauer J and Pinter G. On the strain measurement and stiffness calculation of carbon fibre reinforced composites under quasi-static tensile and tension-tension fatigue loads. *Polym Test* 2014; 40: 256–264.